eLife

Reviewed Preprint
v2 • August 13, 2024
Revised by authors

Reviewed Preprint
v1 • April 26, 2024

Neuroscience

High Frequency Terahertz Stimulation Alleviates Neuropathic Pain by Inhibiting the Pyramidal Neuron Activity in the Anterior Cingulate Cortex of mice

Wenyu Peng, Pan Wang, Chaoyang Tan, Han Zhao, Kun Chen, Huaxing Si, Yuchen Tian, Anxin Lou, Zhi Zhu, Yifang Yuan, Kaijie Wu, Chao Chang, Yuanming Wu, Tao Chen

Department of Biochemistry and Molecular Biology, School of Basic Medicine, The Fourth Military Medical University, 710032 Xi'an, China • Department of Anatomy, Histology and Embryology and K.K. Leung Brain Research Centre, The Fourth Military Medical University, 710032 Xi'an, China • Laboratory of Optical Technology and Instrument for Medicine, Ministry of Education, College of Optical-Electrical and Computer Engineering, University of Shanghai for Science and Technology, 200093 Shanghai, China • Innovation Laboratory of Terahertz Biophysics, National Innovation Institute of Defense Technology, 100071 Beijing, China • Information Materials and Intelligent Sensing Laboratory of Anhui Province, Anhui University, 230601 Hefei, China • School of Electronic and Information Engineering, Anhui University, 230601 Hefei, China • School of Physics, Peking University, 100871 Beijing, China

Abstract

Neuropathic pain (NP) is caused by a lesion or disease of the somatosensory system and is characterized by abnormal hypersensitivity to stimuli and nociceptive responses to non-noxious stimuli, affecting approximately 7–10% of the general population. However, current first-line drugs like non-steroidal anti-inflammatory agents and opioids have limitations, including dose-limiting side effects, dependence, and tolerability issues. Therefore, developing new interventions for the management of NP is urgent. In this study, we discovered that the high-frequency terahertz stimulation (HFTS) at approximate 36 THz effectively alleviates NP symptoms in mice with spared nerve injury. Computational simulation suggests that the frequency resonates with the carbonyl group in the filter region of Kv1.2 channels, facilitating the translocation of potassium ions. *In vivo* and *in vitro* results demonstrate that HFTS reduces the excitability of pyramidal neurons in the anterior cingulate cortex through enhancing the voltage-gated K^+ and also the leak K^+ conductance. This research presents a novel optical intervention strategy with terahertz waves for the treatment of NP and holds promising application in other nervous system diseases.

eLife assessment

Peng et al. reported **important** findings that 36THz high-frequency terahertz stimulation (HFTS) could suppress the activity of pyramidal neurons by enhancing the conductance of voltage-gated potassium channels. The significance of the findings in this paper is that chronic pain remains a significant medical problem, and there is a need to find non-pharmacological interventions for treatment. The authors present **convincing** evidence that high-frequency stimulation of the anterior cingulate cortex can alter neuronal activity and improve sensory pain behaviors in mice.

https://doi.org/10.7554/eLife.97444.2.sa4

Introduction

Neuropathic pain (NP) refers to a debilitating chronic pain condition, which is often a consequence of nerve injury or of the diseases such as cancer, diabetes mellitus, infection, autoimmune disease, and trauma ([1], [2]). The symptoms of NP include spontaneous pain, hyperalgesia and mechanical allodynia. Unfortunately, NP is often resistant to currently available drug treatments, including non-steroidal anti-inflammatory drugs and even opioids ([3]). More evidences reveal that NP is not merely a symptom of a disease but rather an expression of pathological operations of the nervous system ([4]). Therefore, developing new therapeutic technology aimed at these underlying mechanisms for pain relief represents a considerable challenge.

Compared with the limitations of chemical-based drugs research, physics-based treatment offers a new concept and opportunity for intervening in NP. Optogenetics, as an interdisciplinary approach, has demonstrated therapeutic potential in NP. However, the limitations of viral vector delivery systems in humans are well-known ([5]). Recently, evidence has emerged suggesting that high frequency terahertz (THz) photons directly resonate with molecules, thereby regulating corresponding biological functions. For instance, our previous study demonstrated that a 34.88 THz wave resonates with Aβ protein, disrupting the process of fibril formation ([6]). Li et al. discover that the band of 42.55 THz resonates with the stretching mode of either the –COO- or the –C=O group significantly enhancing the Ca^{2+} conductance ([7]). Zhu et al. conclude that 48.2 THz photons greatly increase the permeability of sodium channel by a factor of 33.6 through breaking the hydrated hydrogen bonding network between the hydrosphere layer of the ions and the carboxylate groups ([8]). Additionally, the frequency of 53.5 THz has been reported to enhance the voltage-gated K^+ currents, which modulate the startle response and associative learning ([9], [10]). These studies strongly prompt us the potential application of THz photons in the treatment of neuropathic pain by targeting the ion channels ([11]).

The anterior cingulate cortex plays a crucial role in pain regulation ([12]). Our previous research has demonstrated that nociceptive information resulting from nerve injury is transmitted to the ACC ([13]). This region exhibits pre- and postsynaptic long-term plasticity (LTP), which contributes to chronic pain and associated negative emotions ([14], [15]). Furthermore, descending projection pathways from the ACC enhance the neuronal activity of the spinal dorsal horn (SDH) and regulate nociceptive sensory transmission ([16]). Brain-imaging and MRI studies also provide evidence of hyperexcitability in the ACC during both acute and chronic pain ([17], [18]). Specifically, the activity of pyramidal cells in the ACC is directly correlated with the expression of chronic pain

(19, 20). Optogenetic excitation of ACC pyramidal cells induces pain, while their inhibition leads to analgesia (21). Therefore, targeting the cortical regions of the ACC and inhibiting the activity of ACC pyramidal neurons may hold promise as a strategy for treating NP (22–25).

Neuronal excitability is influenced by various types of voltage-gated ion channels and among them, voltage-dependent potassium (Kv) channels, as one of the important physiological regulators of neuronal membrane potentials, has been proposed as potential target candidates for pain therapy (26–28). Zhao et al. have reported that enhancing Kv currents in injured dorsal root ganglion (DRG) neurons alleviates neuropathic pain (29). Additionally, Fan et al. have demonstrated that lumbar $(L)_5$ spinal nerve ligation (SNL) leads to a time-dependent decrease in Kv1.2-positive neurons in the ipsilateral L_5 DRG. However, rescuing Kv1.2 expression in the injured L5 DRG attenuates the development and persistence of pain hypersensitivity (30). These findings highlight the potential of targeting Kv channels as a therapeutic approach for managing pain.

In this study, we investigated the effects of high-frequency terahertz stimulation (HFTS) on the Kv model. By analyzing the absorbance spectra of Kv1.2 channels, we observed a significant response to photons with a frequency of approximately 36 THz. This frequency modulates the resonance of the carbonyl group in the Kv1.2 structure, affecting the action potential waveform and frequency as demonstrated through simulations. Subsequently, we conducted *in vivo* multi-channel recordings and *in vitro* patch recordings to confirm the activation effect of HFTS on K^+ conductance and its inhibition of neuronal activity in the ACC pyramidal cells. Importantly, the application of HFTS resulted in a significant reduction in pain behavior in mice with spared nerve injury (SNI).

Results

HFTS attenuates the generation of action potential through molecular dynamics simulation

To identify a specific terahertz (THz) frequency capable of modulating a major subset of voltage-gated potassium (Kv) channels, we developed an integrated model comprising both mouse Kv channels (Protein Data Bank [PDB] ID: 3LUT) and Na^+ channels (PDB ID: 3RVY) (**Fig. 1a** and Supplement Fig. S1). We conducted a comprehensive analysis of the spectral absorption characteristics within the THz frequency range. Our results revealed a pronounced absorption peak at approximately 36 THz for the potassium channel, which exhibited a considerable board band compared to the absence of a corresponding peak for the sodium channel (**Fig. 1a**). This indicates a preferential and resonant absorption of photons at the ~36 THz frequency by the potassium channel. We then tested the possible kinetic changes of Kv1.2, the typical and widely distributed Kv channel in the central nervous system (31), following the absorption of these THz photons. Our findings indicated a significant kinetic change in the -C=O groups of the channel filter structure, as evidenced by an expansion of its van der Waals radius by approximately 0.5 Å (**Fig. 1b**). Furthermore, during exposure to THz photons, the conductance of the potassium ion channel exhibited an almost linear increase with the intensity of the THz field, while the conductance of sodium ions remained largely unchanged (**Fig. 1c**). Interestingly, under terahertz photonic influence, the cortical neurons model showed significantly decreased in discharge (**Fig. 1d**). We performed a detailed waveform analysis of the action potentials, including parameters such as full width at half maximum (FWHM) and firing frequency (**Fig. 1e**). Our observations revealed that the FWHM of action potentials in the THz-exposed group decreased to 95% of the control group (**Fig. 1f**, red column), and the firing frequency experienced a reduction of approximately 70% after THz photon stimulation (**Fig. 1f**, green column). These results collectively suggest that THz photons primarily attenuate neuronal firing activity by increasing potassium ion conductance, thereby modulating neuronal excitability.

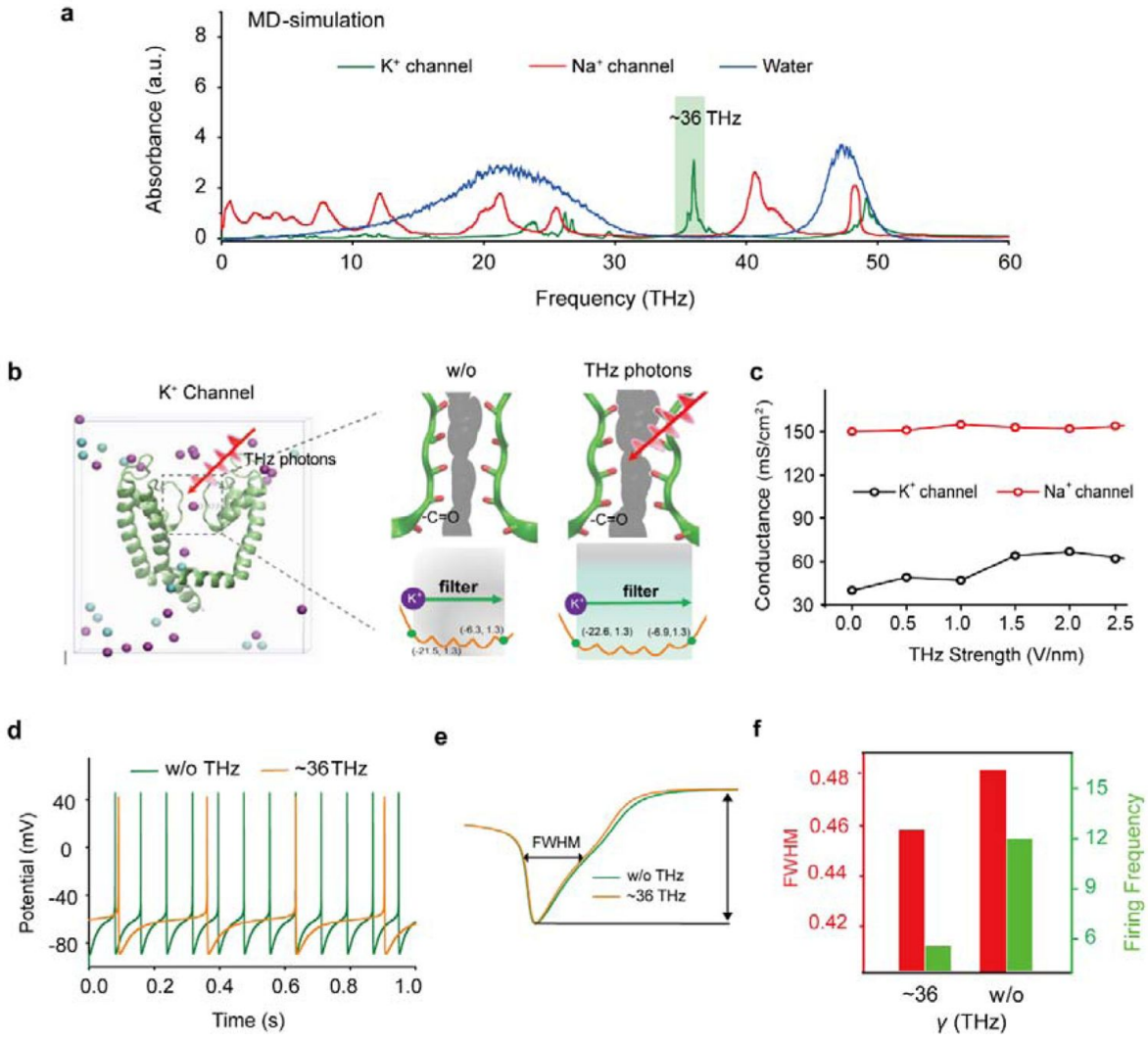

Fig. 1

Specific frequency THz photons resonate K_V channel and decrease the AP firing rate in cortical neurons through molecular dynamics simulation. (a) Absorbance spectra of voltage-gated potassium/sodium ion channels and the bulk water. (b) The dynamic attributes of the Kv1.2 filter structure in pre- and post-exposure to HFTS. Purple balls represent the K^+, blue balls represent the Cl^-. (c) The alterations in potassium/sodium ion conductance consequent to the influence of HFTS. (d) Changes of the firing rate of APs of cortical neuron models before and after HFTS. (e) The FWHM of an AP pre- and post HFTS. (f) Changes in FWHM and firing frequency with or without HFTS. HFTS, high frequency terahertz stimulation. AP, action potential. FWHM, Full Wide of Half Maximum.

HFTS enhances voltage-gated K^+ currents and leak K^+ currents of pyramidal neurons in the ACC

To investigate the impact of high-frequency terahertz stimulation (HFTS) on voltage-gated potassium/sodium (Kv/Nav) channels, which play a crucial role in action potential generation and waveform, we conducted whole-cell patch recording from layer-5 pyramidal neurons (PYR^{ACC}) in acute slices of anterior cingulate cortex (ACC) in mice with spared nerve injury (SNI) (**Fig. 2a**). Initially, we examined the Nav current by applying a series of test pulses (from −80 to −10 mV) with a command voltage of −100 mV (20 ms) (**Fig. 2b**). Upon illumination with ~36 THz photons (0.3 ± 0.05 mW) for durations of 5, 10 and 20 minutes, we observed that HFTS had no significant effect on the activation and inactivation curve slope, half-activation and half-inactivation voltage and time constants (tau) for half-activation and half-inactivation voltage (**Figs. 2c-f**). These findings indicate that HFTS does not affect Nav channel-mediated currents. Subsequently, we investigated the influence of HFTS on Kv currents by applying a series of test pulses (100 ms) ranging from −70 to +130 mV with a command voltage of −100 mV (**Fig. 2g**). Our results demonstrated that the application of HFTS induced a significant increase in the amplitude of K^+ currents (Table S1-1) and an enhanced slope of the current-voltage characteristic (I-V) curve (**Figs. 2h-j**), without affecting the half-activation voltage (**Fig. 2k**). Furthermore, to assess the duration of neuronal effects induced by HFTS (15 minutes), we examined Kv currents at 5 minutes and 20 minutes post-HFTS. It was observed that the Kv current were enhanced 20 minutes post-HFTS (**Fig. 2l**, Table S1-2). Simultaneously, we studied the effect of HFTS on K_{Leak} currents by applying a series of test pulses (400 ms) ranging from −120 to −30 mV followed with a command voltage of −70 mV (**Fig. 2m**). Currents recorded at and above −65 mV membrane potential were analyzed for potential K_{Leak} currents ([32]). We found that HFTS also induced a significant increase of K_{Leak} currents at holding potential at −40 and −30 mV (**Fig. 2n**) (Table S1-3). These experiments demonstrated that HFTS at approximately 36 THz not only influenced Kv currents but also affected K_{Leak} channel activity, resulting in an acceleration of potassium ion flow and an increase in potassium conductance in PYR^{ACC} neurons. Importantly, these experimental findings were consistent with the results obtained from molecular dynamics analysis.

HFTS reduces the spike frequency of pyramidal neurons in the ACC

We proceeded to investigate the impact of the specific resonant frequency of THz photons on the excitability of PYR^{ACC} neurons in SNI and sham mice. Using whole-cell current-clamp recording, we compared the input-output curves of evoked action potentials before and after HFTS. Our findings revealed a significant increase in the spike frequency in SNI mice (**Fig. 3a**) (Table S2-1), which was effectively rescued by the application of HFTS (**Fig. 3b**) (Table S2-2), but not by 465 nm blue light stimulation (BLS) (**Fig. 3c**) (Table S2-3). Furthermore, the spike frequency in sham mice also decreased after the application of HFTS (**Fig. 3d**) (Tables S2-4). To further analyze the properties of single action potentials, we induced them by applying a depolarizing current pulse (30 ms) of an appropriate suprathreshold magnitude (**Fig. 3e**). In SNI mice, we observed a decrease in the rheobase and an elevation in the resting membrane potential (RMP) compared to those in sham mice. However, these alterations were reversed by the application of HFTS, while BLS had no effects. Other parameters, such as voltage threshold, amplitude and half-width of the action potentials, were not different between SNI or sham mice with and without HFTS (**Figs. 3f-k**). Given that the spike firing, rheobase and RMP are closely related to low-threshold Kv channels and K_{Leak} channels ([26], [31], [33]), these results suggest that HFTS affects the activity of PYR^{ACC} neurons through its specific impact on Kv and K_{Leak} channels.

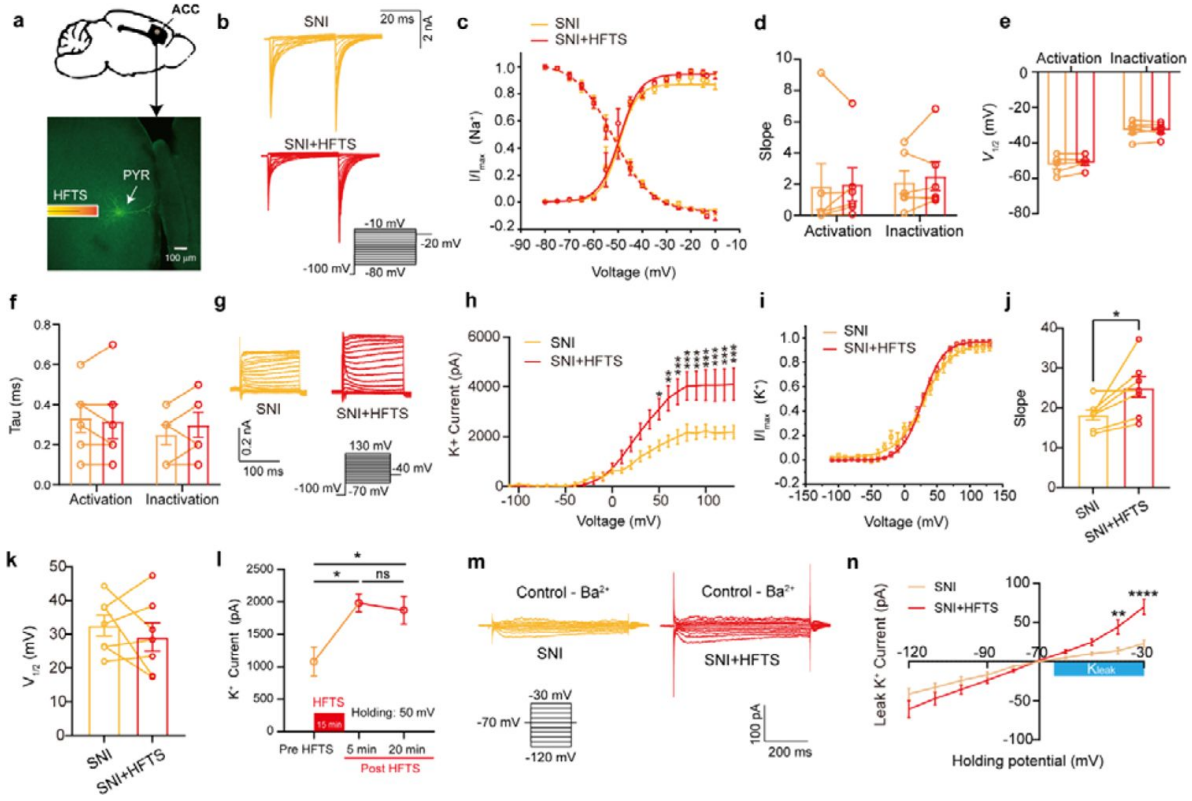

Fig. 2

HFTS enhances Kv and K_{Leak} currents of pyramidal neurons in SNI mouse *in vitro*. (a) Anatomical location of ACC region in mice and a recorded PYR neuron (biocytin-labeled, green). (b) Representative Nav currents without (orange) or with HFTS (red) under the given step voltage protocol. (c) The activation and inactivation curves of Nav currents with and without HFTS. (d-f) The corresponding slopes of the activation and inactivation curves (d), the comparison of the half-activation and inactivation voltages (e) and the time constants (tau) of half-activation voltage/half-inactivation voltage (f). (g) Representative Kv currents evoked by a series of step voltages (inset) without (orange) or with HFTS (red). (h) I-V plots constructed from the values of traces shown in (g). (SNI *vs.* SNI + HFTS: $F_{(1, 10)} = 6.846$, $P < 0.0001$, $n_{SNI} = 6$, $n_{SNI+HFTS} = 6$; Two-way ANOVA followed by *post hoc* comparison using the Šídák's multiple comparisons test). (i) The activation curves of the Kv currents with and without HFTS. (j) The corresponding slopes of the activation curves (SNI *vs*. SNI + HFTS: $t = 5.872$, $P = 0.0011$, n = 7, unpaired *t*-test. **, $P < 0.01$, ****, $P < 0.0001$). (k) the half-activation voltages of the activation curves. (l) Changes in the impact of Kv current post-HFTS. ($F_{(4, 15)} = 4.19$, $P = 0.0178$, n = 4; One-way ANOVA followed by *post hoc* comparison using the Šídák's multiple comparisons test). (m) Representative K_{Leak} currents evoked by a series of step voltages (inset) without (orange) or with HFTS (red). (n) I-V plots constructed from the values of traces shown in (m). (SNI *vs.* SNI + HFTS: $F_{(1, 12)} = 1.688$, $P = 0.2182$, $n_{SNI} = 7$, $n_{SNI+HFTS} = 7$; Two-way ANOVA followed by *post hoc* comparison using the Šídák's multiple comparisons test).

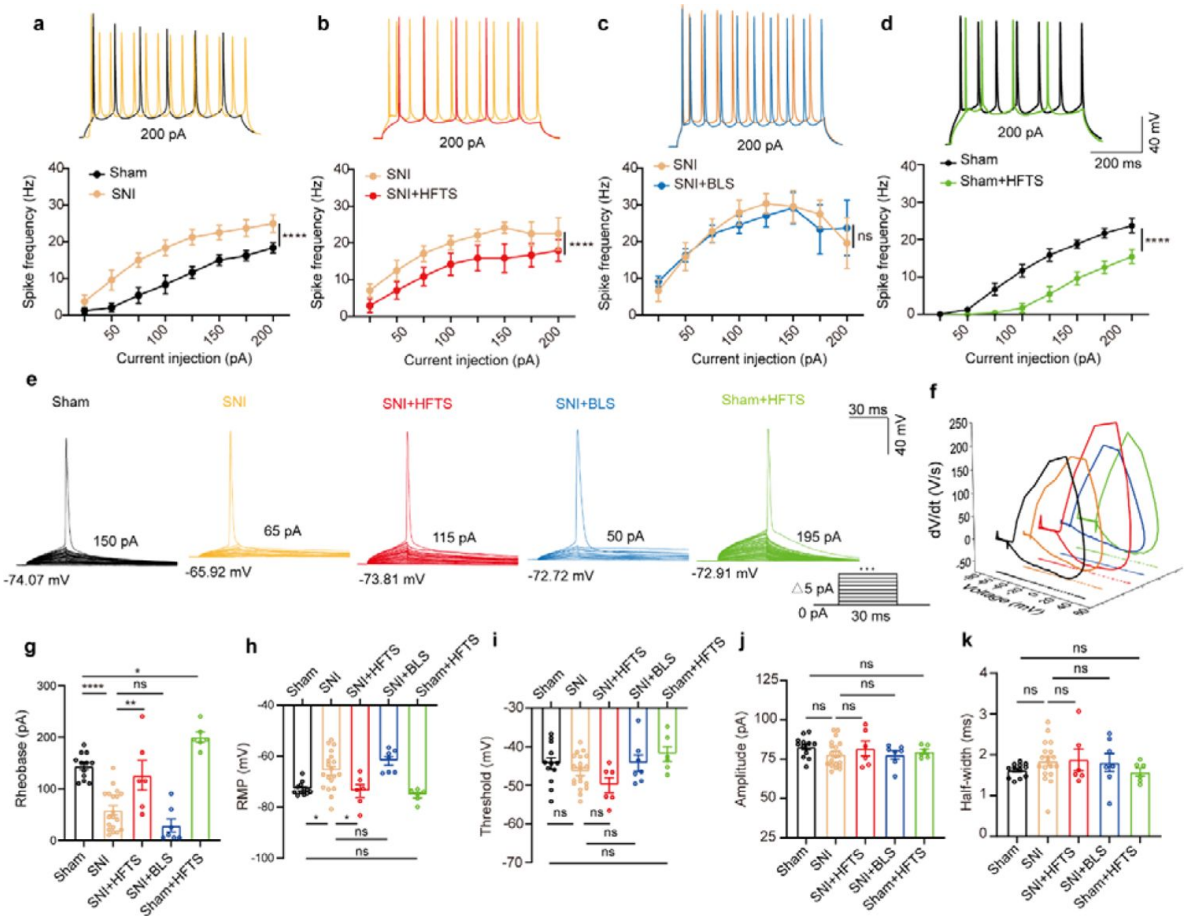

Fig. 3

HFTS reduces the APs firing rate of pyramidal neurons in SNI and sham mice *in vitro*. (a-d) Representative traces (upper panels) and line-charts (lower panels) showing the changes of evoked spikes of pyramidal neurons in different groups. (Sham *vs*. SNI: $F_{(1, 40)}$ = 124.2, P < 0.001, n_{sham}= 6, n_{SNI}=6; SNI *vs.* SNI + HFTS: $F_{(1, 40)}$ = 23.13, P < 0.0001, n_{SNI}=6, $n_{SNI+HFTS}$=6; SNI *vs.* SNI + BLS: $F_{(1, 40)}$ = 0.1401, P = 0.7101, n_{SNI} = 6, $n_{SNI+BLS}$ = 6; Sham *vs.* Sham + HFTS: $F_{(1, 40)}$ = 87.29, P < 0.0001, n_{Sham} = 6, $n_{Sham+HFTS}$ = 6. Two-way ANOVA followed by *post hoc* comparison using the Šídák's multiple comparisons test). (e) Superimposed traces showing the single AP evoked by threshold current stimulation in different groups. (f) Phase plots of AP traces in each groups. (g) Histograms showing the statistical comparison of rheobase in each group. (Sham *vs*. SNI: q = 8.456, P < 0.0001, n_{sham} = 12, n_{SNI} = 19; SNI *vs.* SNI + HFTS: q = 5.264, P < 0.01, n_{SNI} = 19, $n_{SNI+HFTS}$ = 6; Sham *vs.* Sham + HFTS: q = 4.098, P < 0.05, n_{SNI} = 19, $n_{SNI+HFTS}$ = 6. one-way ANOVA followed by *post hoc* comparison using the Tukey's multiple comparisons test). (h) The RMP in each group (Sham *vs.* SNI: q = 4.887, P < 0.05, n_{sham} = 12, n_{SNI} = 19; SNI *vs.* SNI + HFTS: q = 4.29, P < 0.05, n_{SNI} = 19, $n_{SNI+HFTS}$= 6; Sham *vs.* Sham + HFTS: q = 1.261, P > 0.05, n_{SNI} = 19, $n_{SNI+HFTS}$ = 6. one-way ANOVA followed by *post hoc* comparison using the Tukey's multiple comparisons test). (i-k) HFTS has no significant effect on the threshold, amplitude and half-width of APs in pyramidal neurons.*, P < 0.05, **, P < 0.01, ***, P < 0.001, ****, P < 0.0001, ns, P > 0.05. BLS, blue light stimulation.

HFTS decreases the excitability of pyramidal neurons in the ACC *in vivo*

We then investigate the effect of HFTS on the activities of PYR^{ACC} in head-fixed awake SNI mice. One-week prior to the illumination experiment, a 16-channel electrode was implanted into the ACC (the detailed structure of this device shows in **Fig. 4a**). Then we applied THz photon stimulation for 15 minutes and compared the neuronal activities before and after HFTS (**Fig. 4b**). Our findings revealed a significant decrease in the mean firing rate of ACC neurons after HFTS application in both the sham and SNI groups (**Figs. 4c and g**). To further analyze the effect of HFTS on the PYR^{ACC}, we classified them along with interneurons in the ACC (INT^{ACC}) based on their firing rate, trough-to-peak duration and half width (**Fig. 4d**), as described in our previous study ([19]). We assessed the internal-spiking interval (ISI) and waveform characteristics of the isolated neurons in each channel to ensure that the pre- and post-HFTS units originated from the same neuron (**Fig. 4e**). In the sham group, we observed that 63.4% of PYR^{ACC} neurons exhibited a decrease in firing rate, 10.8% of PYR^{ACC} showed an increase, and 25.8% of PYR^{ACC} remained unchanged (93 well-isolated PYR^{ACC} neurons were recognized out of 108 total recorded units). In the SNI group, we found that 61.8% of PYR^{ACC} neurons exhibited decreased activity, 20.3% of PYR^{ACC} showed increased activity, and 17.9% of PYR^{ACC} remained unchanged (123 well-isolated PYR neurons were recognized out of 130 total recorded units) (**Fig. 4f**). Consistently, the increased mean firing rate of PYR^{ACC} neurons in SNI mice was significantly inhibited by the application of HFTS (**Fig. 4h**). The activity of INT^{ACC} also tended to decrease after HFTS (**Fig. 4i**). In contrast, blue light stimulation (BLS) has no effect on the mean firing rate on the PYR^{ACC} and INT^{ACC} in both sham and SNI mice (Supplement Fig. S2). These results indicate that HFTS reduces the spike firing of ACC neurons, whereas BLS does not have the same effect.

HFTS alleviates mechanical allodynia of SNI mice

Finally, we tested whether application of HFTS into the ACC induced analgesic effects. The SNI surgery and optic fiber tube implantation into the ACC were performed one week before pain behavioral tests, which included the mechanical pain threshold test and Catwalk analysis (**Fig. 5a**). We compared the paw withdrawal mechanical thresholds (PWMTs) before and after HFTS (0.3 ± 0.05 mW at the tip of the optic fiber) application for 15 minutes and found that SNI treatment significantly decreased the PWMTs compared to the sham group. However, after the application of HFTS, the PWMTs significantly increased, even surpassing those in the sham group in the first 30 minutes (**Fig. 5b**). The analgesic effect lasted for around 160 minutes with a 15-minute application of HTFS and lasted for around 140 minutes with a 10-minute application of HTFS, suggesting a correlation between the duration of analgesia and the intensity of stimulation (**Fig. 5c**). In contrast, the PWMTs did not significantly change in the SNI group with the application of 465 nm blue light.

Furthermore, we performed the Catwalk gait analysis (**Figs. 5d-l**), which provides exquisite and reliable observations for evaluating the spontaneous pain behaviors ([34]). We focused on the print intensity and print area related parameters of the left hind paw (ipsilateral side of the injured nerve). We found that SNI treatment significantly altered the stand time, the stand index, the max contact area, the mean print area, the mean intensity and the duty cycle (**Figs. 5g-l**). This suggests that the SNI mice tend to avoid standing and walking on their injured hind paw due to pain hyper-sensitivity. The application of HFTS but not BLS rescued most of the above parameters, indicating HFTS' strong analgesic effect.

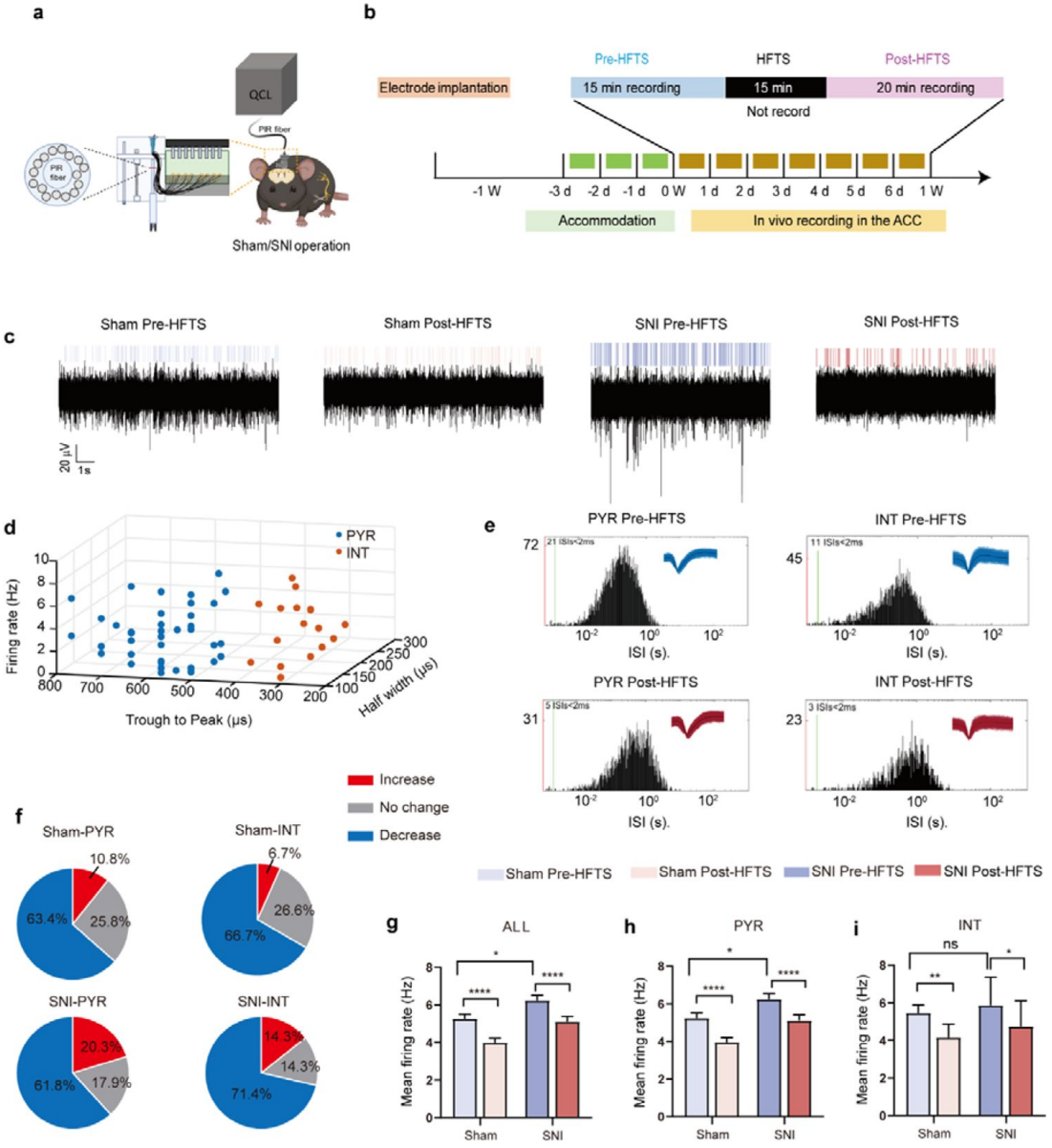

Fig. 4

HFTS decreases the mean firing rate of pyramidal neurons in the ACC in both sham and SNI awake mice. (a) Schematic diagram of the single-unit recording of the ACC using an *in vivo* multi-channel recording technique. (b) The timeline and the stimulating pattern of HFTS on an awake mouse. (c) Example recording signals of ACC neurons before and after HFTS application in sham and SNI groups, respectively. (d) ACC neurons are classified as pyramidal (PYR) cells and interneurons (INT) using *k*-means cluster-separation algorithm based on their electrophysiological properties. (e) Histograms of the inter-spike intervals (ISI) from the spikes of a PYR and an INT in pre- and post-HFTS recording period. Insets at the top right corner show the waveforms of the detected single unit. (f) Pie charts summarize the changes in firing rate of PYR and INT in sham and SNI groups. Pre *vs.* post HFTS, Wilcoxon rank-sum test. (g) The mean firing rate of all recorded neurons in sham and SNI groups before and after HFTS. Sham group ($P < 0.0001$, n = 108, Wilcoxon matched-paired signed rank test), SNI group ($P < 0.0001$, n = 130, Wilcoxon matched-paired signed rank test), SNI pre-HFTS vs. Sham pre-HFTS ($P = 0.0447$, Mann-Whitney test). (h) The mean firing rate of PYR neurons in sham and SNI groups before and after HFTS. Sham group ($P < 0.0001$, n = 93, Wilcoxon matched-paired signed rank test), SNI group ($P < 0.0001$, n = 123, Wilcoxon matched-paired signed rank test), SNI pre-HFTS vs. Sham pre-HFTS ($P = 0.0274$, Mann-Whitney test). (i) The mean firing rate of INT neurons in sham and SNI groups before and after HFTS. Sham group ($P = 0.0084$, n = 15, Wilcoxon matched-paired signed rank test), SNI group ($P = 0.0313$, n = 7, Wilcoxon matched-paired signed rank test), SNI pre-HFTS vs. Sham pre-HFTS ($P = 0.3322$, Mann-Whitney test). *, $P < 0.05$, **, $P < 0.01$, ****, $P < 0.0001$, ns, $P > 0.05$.

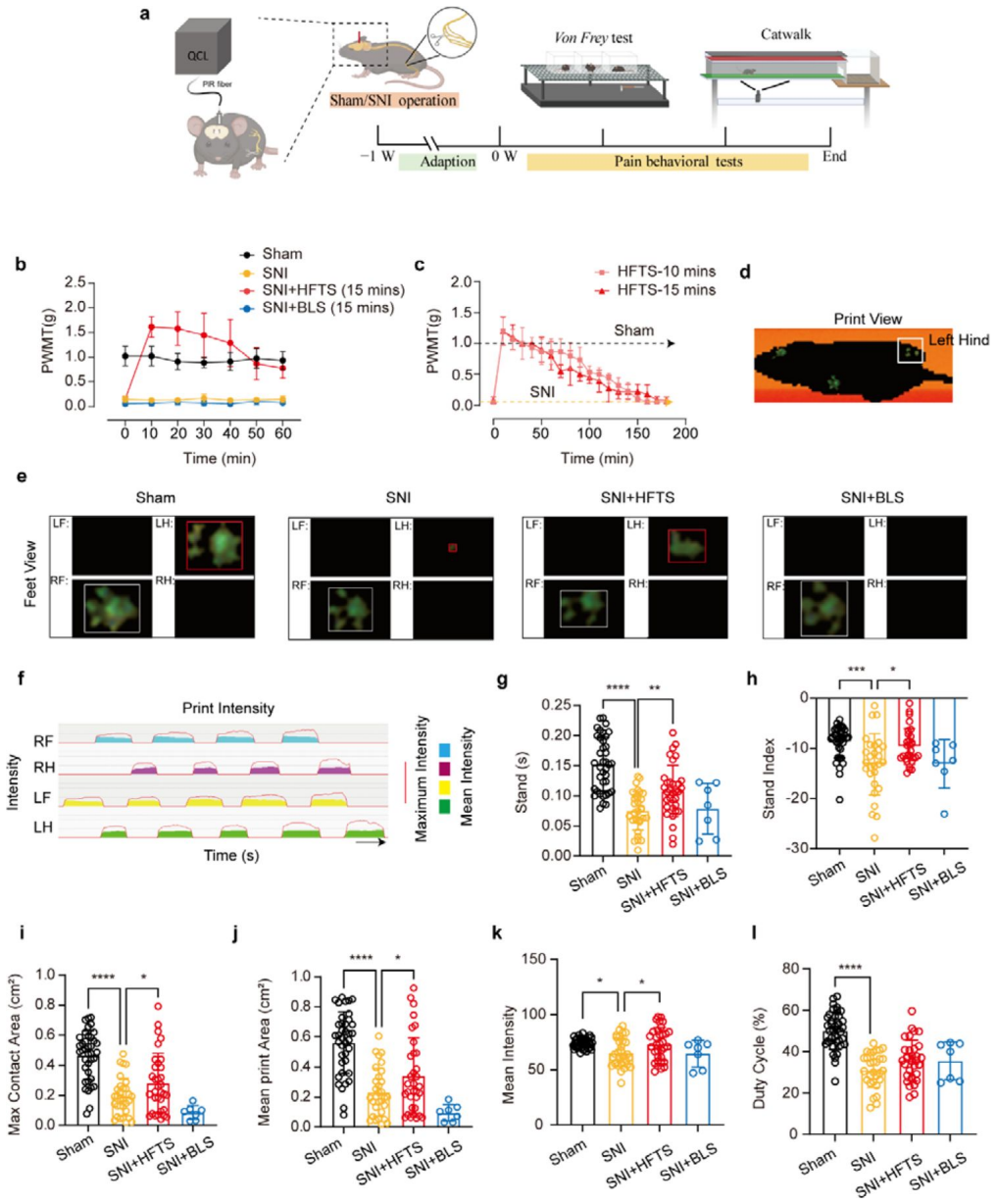

Fig. 5

HFTS alleviates neuropathic pain of SNI mice through pain behavior tests. (a) Schematic of the establishment of NP model, the application of HFTS in ACC region and the following behavior tests including *Von Frey* test and Catwalk analysis. (b) HFTS increases the paw withdrawal mechanical thresholds (PWMTs) compared to the SNI model ($F_{(18, 140)}$ = 12.65. P < 0.0001. Sham *vs.* SNI: P < 0.0001; SNI *vs.* SNI + HFTS: P < 0.0001; n = 6 in each group. Two-way ANOVA repeated measures followed by *post hoc* comparison using the Šídák's multiple comparisons test). (c) Duration of the analgesic effect with HFTS for 10 mins and 15 mins. (d) The print view of a mouse. (e) The feet view of the left front (LF), left hind (LH), right front (RF) and right hind (RH) in the groups of sham, SNI, SNI + HFTS and SNI + BLS, respectively. (f) The step sequence of a sham mouse who passing through the glass pane, the red line represents the maximum intensity of each foot, the color box represents the mean intensity of the corresponding print during walking. (g) HFTS increases the LH stand time of SNI mice (sham *vs.* SNI: P < 0.0001; SNI *vs.* SNI + HFTS: P < 0.01). (h) HFTS increases the LH stand index of SNI mice (sham *vs.* SNI: P < 0.001; SNI *vs.* SNI + HFTS: P < 0.05). (i) HFTS increases the LH max contact area of SNI mice (sham *vs.* SNI: P < 0.0001; SNI *vs.* SNI + HFTS: P < 0.05). (j) HFTS increases the LH mean print area of SNI mice (sham *vs.* SNI: P < 0.0001; SNI *vs.* SNI + HFTS: P < 0.05; SNI vs. SNI + BLS: P < 0.05). (k) HFTS increases the LH mean intensity of SNI mice (sham *vs.* SNI: P < 0.05; SNI *vs.* SNI + HFTS: P < 0.05). (l) HFTS have no significant for the pain behavior parameter of the duty cycle. *, P < 0.05, **, P < 0.01, ***, P < 0.001, ****, P < 0.0001. One-way ANOVA (f-k) followed by *post hoc* comparison using the Tukey's multiple comparisons test. n_{Sham} = 38, n_{SNI} = 35, $n_{SNI+HFTS}$= 34, $n_{SNI+BLS}$ = 9.

Discussion

In the present study, we provide evidence that high frequency terahertz photons alleviate neuropathic pain in the SNI mice by decreasing the excitability of pyramidal neurons in the ACC. The mechanism underlying this effect is that HFTS increases voltage-gated potassium ion conductance through resonance with the carbonyl group in the potassium channel filter region (**Fig. 6**). Unlike optogenetic technology, HFTS can directly regulate the conformation of ion channel without delivering a transgene that encodes a light-response protein. It exhibits frequency selectivity and dependence to channel structure. This research suggests that HFTS has potential to serve as a novel optical technology for the treatment of NP pathology.

Neuropathic pain is closely associated with nociceptor excitability in the ACC ([18], [35]-[37]), with ion channels playing a fundamental role in determining neuronal excitability, particularly in the hyperexcitability of pyramidal neurons ([11]). Excitatory Nav channels, responsible for initiating and depolarizing the action potential, can be targeted by inhibitors to effectively decrease or eliminate electrical excitability. These inhibitors are commonly used in neurology as antiepileptic drugs. On the other hand, inhibitory K channels, responsible for repolarization, contribute to the initiation of action potentials in diverse ways ([33]). Enhancing K conductivity could have a similar effect to Nav channel blockers. For instance, retigabine, an activator for Kv7, has recently been approved as a first-in-class antiepileptic drug ([38], [39]). Among the 12 subfamilies of Kv channels (Kv1-12), Kv1.2 is the most prevalent in neuronal membranes([40]) and has been reported to be significant associated with neuropathic pain ([30], [41], [42]). Although the response frequency of Kv1.2 at ~53 THz ([10]) or ~34 THz ([43]) and the corresponding modulation function have been verified due to the broad absorption band, this study highlights the significant resonance of Kv1.2 filter structure with photons at 36 THz. By optically stimulating ACC neurons with the frequency of ~36 THz, we observed a significant reduction in the firing rate of pyramidal neurons' action potentials in SNI mice, accompanied by a notable enhancement of K^+ conductance. This confirms the effect of THz photons on Kv channels, including Kv1.2. However, to consolidate this conclusion, a more specific pharmacological experiment is necessary. For example, applying a blocking peptide to eliminate the Kv1.2 current and then testing whether this blocks the effects of HTFS would be a valuable test to perform in the future. Moreover, the application of HFTS resulted in significant changes in the rheobase and RMP of pyramidal cells, suggesting that HFTS may also affect the two-pore K^+ channels ([31]). We thus tested the effect of HTFS on the K_{leak} current and confirmed this hypothesis. Additionally, it has been reported that basal excitability is influenced by the opening of low-threshold Kv1.2 channels, which filter out small depolarizations and thus control the number of triggered APs ([40]). However, we cannot exclude the possibility that THz photons affect other K channel functions, but further research is required to confirm this in the future.

During our research, we focus on studying of pyramidal neurons in the ACC ([44]). It has been reported that the firing rate of glutamatergic pyramidal cells, rather than inhibitory interneurons, increases in the ACC after chronic pain, suggesting an imbalance of excitatory/inhibitory (E/I) ratio ([19], [35]). In the local circuits of the ACC, inhibitory neurons release GABA and inhibit the activities of pyramidal cells. Different studies by Kang et al.([45]) and Joseph Cichon et al.([46]) have reported that specific activation of interneurons in the ACC or in the somatosensory cortex reduces pyramidal neuron hyperactivity and alleviate mechanical allodynia. Thus, the application of THz may induce complicated results through affecting the Kv channels distributed on both pyramidal cells and interneurons. However, as shown in our *in vivo* recording data (**Fig. 4i**), although THz illumination slightly decreased the activity of interneurons, which could potentially lead to an enhanced activity of local pyramidal cells, the direct and significant decrease in

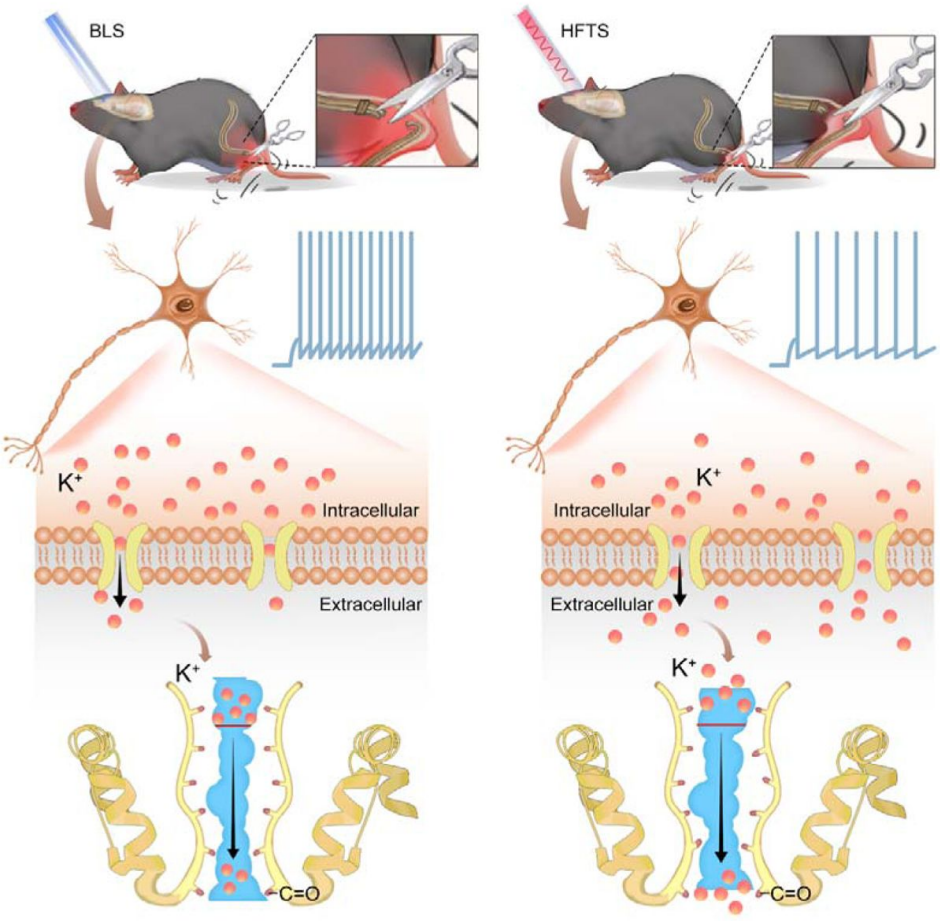

Fig. 6

Schematic diagram shows the mechanism of HFTS in alleviating neuropathic pain. Left panel shows the group with BLS and the right panel shows the group with HFTS.

pyramidal cell activity caused by the illumination would overcome this disinhibitory effect, ultimately resulting in a net decrease in pyramidal cell activity. The behavioral analgesic effect caused by THz illumination also confirmed this conclusion.

There are several limitations in this study that should be acknowledged. Firstly, we did not investigate the thermal effect of HFTS on the Kv channel. Previous research has demonstrated the non-thermal, long-distance stimulation of high-frequency terahertz stimulation on neuronal activity ([10]). Nevertheless, the specific interaction between ~36 THz and Kv channels in terms of thermal effects remains unexplored. Additionally, in this study, we used blue light as a comparison, and found no significant changes in potassium current and the excitability of pyramidal cells. This finding suggests the specificity of the terahertz frequency and supports the existence of non-thermal effects. Another limitation of our research is the use of an optic fiber to deliver the HFTS into the ACC region. This invasive approach may pose challenges for potential noninvasive applications. However, we believe that with the advancement of terahertz enhancement techniques, such as the use of metasurfaces or nanomaterials ([47], [48]), high-frequency terahertz waves show promising potential for broad applications in regulating diverse brain diseases, such as episodic ataxia ([38], [49]), benign familial neonatal convulsions ([50]), Alzheimer's disease ([51]), and others.

Material and methods

Animals

Male adult (8–10 weeks) C57BL/6 were used for all experiments. Mice were housed on a 12 h light–dark cycle with food and water freely available. The living conditions were carefully controlled, with temperatures maintained at 22-26℃ and humidity at 40%. All animal procedures in the present experiments were in accordance with protocols approved by the Animal Care Committee of the Fourth Military Medical University. All efforts were made to minimize animal suffering and the number of animals used.

Neuropathic Pain Model

We used spared nerve injury (SNI) model to establish neuropathic pain. The detailed process has been described in our previous study ([19]). In brief, mice were generally anaesthetized by 2% isoflurane. Three terminal branches of the left sciatic nerve were exposed by making a direct incision in the skin and a section of the biceps femoris muscle in the left thigh. The tibial nerve and the common peroneal nerve were ligated using 6-0 silk sutures and then sectioned distal to the ligation. After ligating and cutting the nerves, they were carefully put back into their original positions, and the muscle and skin were sutured in two layers. For the sham mice, animals only received an operation that exposed the branches of the left sciatic nerve but without any nerve injury. Following a week accommodation period, pain behaviors were assessed using the *von Frey* filament test and CatWalk gait analysis to confirm the successful establishment of the NP model.

Molecular Dynamics Simulation

The simulation was conducted to gain a deeper understanding of the interaction between terahertz photons and ion channels. A composite model of mouse eukaryotic voltage-gated K^+ channels (PDB ID: 3LUT) and eukaryotic Na^+ channels (PDB ID: 3RVY) was built using the Charmm-GUI website. The model consisted of intact proteins, phospholipid bilayers, and saline solution (with a concentration of 0.15 M). Kinetic calculations were performed using GROMACS 5.1.2 software. The CHARMM 36 force field and periodic boundary conditions were applied to the proteins. Electrostatic interactions were handled using the connected element algorithm Ewald. During the simulation, the Rattle algorithm was used to constrain key lengths. The motion equation was solved using the Velocity-Verlet algorithm with a time step of 2 fs. Initially, the

simulation was carried out at a room temperature of 303.5 K to observe the ion transport process within the channels at the molecular level. Subsequently, conductivity values (gNa, gK) for potassium and sodium ions and their corresponding absorption spectrum were calculated. To investigate the effect of ion transport under the influence of terahertz radiation, time-varying electric fields of THz radiation were added to the system. In the interaction of terahertz radiation with biological systems, electrical components play a crucial role. The electric field was used to simulate terahertz radiation, and its formula is as follows:

$$E(t) = A \bullet u \bullet \cos(\omega t + phi)$$

Where A represents the terahertz radiation intensity, u and phi represent the polarization direction and phase of the radiated photon, which set to (0, 0, 1) and 0, respectively. The terahertz radiation frequency v is related to the angular frequency ω by the equation:

$$v = \omega / 2\pi$$

The cortical neuron Hodgkin-Huxley (H-H) model links the microscopic level of ion channels to the macroscopic level of currents and action potentials. The model consists of two distinct components: a rapid inward current carried by sodium ions and a slower activating outward current carried by potassium ions. These currents result from independent permeability mechanisms for Na^+ and K^+, where the conductance changes over time and membrane potential. Consequently, the model can replicate and explain a wide range of phenomena, including the shape and propagation of action potentials, the sharp threshold, refractory period, anode-break excitation, accommodation, and subthreshold oscillations. Minor adjustments in key conductance and stimulus current parameters enable the model to describe various action potential phenomena ([52]). The formula shows as follows:

$$C\frac{dv}{dt} = G_{stim} - g_{Na}(THz)\, m^3 h(v - v_{Na}) - g_K(THz)\, n(v - v_K) - g_L n(v - v_L)$$
$$\frac{dy}{dt} = \alpha_y(1 - y) - \beta_y y, \qquad y = m, n$$
$$\frac{dh}{dt} = \left(\frac{1}{1 + \exp((v + 60)/6.2)} - h\right)(\alpha_h + \beta_h),$$

Where v, m, h and n represent the membrane voltage, probability of opening or closing of potassium-sodium ion channel. V_{Na}, V_K and V_L are the sodium ion reverse potential, potassium ion reverse potential and resting membrane potential, respectively. g_{Na}, $g_K$are the maximum conductivity of sodium and potassium ion, respectively. C is membrane capacitive reactance with 0.75 uF/cm^2, the G_{stim} is the stimulation by an external current.

High Frequency Terahertz and Blue Light Stimulation

For high frequency of terahertz stimulation (HFTS), we used a quantum cascade laser with a center frequency of 35.93±0.1 THz. The laser beam was coupled into a coupler, supported by the Innovation Laboratory of Terahertz Biophysics. We then connected the coupler to a Polycrystalline fiber (PIR) infrared fiber (Art photonics) with a core composition of AgCl/Br. This fiber has excellent transmittance in the range of 3-18 μm, with a core refractive index of 2.15 and an effective numerical aperture (NA) of 0.35 ± 0.05. At the distal end of the fiber, we left approximately 3-4 cm of bare fiber to allow for the insertion of a hollow tube with an inner diameter of 650 μm. This tube was pre-implanted into the ACC region of the SNI and sham group mice brain ([53]). The duration of HFTS was 15 minutes, with a pulse width of 2 μs, a repetition frequency of 10 kHz, and a duty cycle of 40%. The average output power at the tip of the fiber, measured by a MIR detector (NOVA II-3A, Israel), was 0.3 ± 0.05 mW. For comparison purposes, we also used a blue laser to stimulate the same brain region for 15 minutes, with a frequency of 1 Hz and an average output power of 10 mW.

In Vitro Patch Clamp Recording

The experimental procedures were based on our previous reports ([54]). Briefly, mice were anesthetized and then decapitated to sacrifice. Brain slices (300 μm thick) containing the ACC were cut on a vibrating microtome (Leica VT 1200s, Heidelberger, Nussloch, Germany) at 0–4°C in oxygenated (95% O_2 and 5% CO_2) artificial cerebrospinal fluid (ACSF) consisting of (in mM) 124 NaCl, 25 $NaHCO_3$, 2.5 KCl, 1 NaH_2PO_4, 2 $CaCl_2$, 1 $MgSO_4$ and 10 glucose. Slices were then transferred to a room temperature-submerged recovery chamber containing oxygenated ACSF and incubated for at least one hour before patch clamp recording. The neurons were then visualized under a microscope with infrared differential interference contrast or fluorescent optics video microscopy (BX51W1, Olympus, Tokyo, Japan). The recording pipettes (3-5 MΩ) were filled with a solution composed of (in mM) 124 K-gluconate, 5 NaCl, 1 $MgCl_2$, 0.2 EGTA, 2 MgATP, 0.1 Na_3GTP, 10 HEPES and 10 phosphocreatine disodium (adjusted to pH 7.2 with KOH, 290 mOsmol). Biocytin (0.2%) were added into pippette solution for verifying neurons and visualized through biocytin-avidin reaction. To examine the properties of voltage-gated K^+ currents, tetrodotoxin (TTX, 1 μM) and $CdCl_2$ (100 μM) were added into the ACSF. $BaCl_2$ (4 mM) were applicated for recording K_{Leak} currents, since barium blocks most K_{Leak} channel subtypes. To examine voltage-gated Na^+ current, 3 mM 4-AP and 0.1 mM $CdCl_2$ were added into the ACSF. Electrical signals were filtered at 1 kHz by a Multiclamp 700B amplifier (Molecular Devices, USA), and digitized by an Axon DigiData 1550A converter with a sampling frequency of 10 kHz. Data analyses were performed with the Clampfit 10.02.

In Vivo Multi-Channel Recording

Before the SNI operation, we implanted an electrode into the right ACC as in our previous reports ([19]), following stereotaxic coordinates: 1.1 mm anterior to the bregma, 0.3 mm lateral to the midline and 1.8 mm vertical to the skull surface. The electrodes were secured to the exposed skull using the dental adhesive resin cement Super-bond C&B (Japan)([53]). This electrode consisted of 16-channel wire electrodes and included a hollow tube. During the optical stimulation, we employed multi-channel recording technology by Neurolego system (Nanjing Greathink Medical Technology, Nanjing, China). Subsequently, single-unit spike sorting was performed using the MClust-v4.4 toolbox in MATLAB software (MathWorks, USA). In the ACC region, the two main cell types are pyramidal neurons and interneuron cells, which are gamma-aminobutyric acid (GABA) neurons. Pyramidal neurons were primarily classified based on a trough-to-peak duration above 430 us, indicating long-duration action potentials. Interneuron cells, on the other hand, were identified based on a duration time below 430 μs ([55]).

Behavioral Assays Mechanical allodynia

Briefly, the paw withdrawal mechanical threshold (PWMT) was evaluated by using von Frey filaments (Stoelting, Kiel, WI, USA) as reported in our previous works ([54]). Mice were habituated to the testing environment for 3 days before baseline testing and then placed under inverted plastic boxes (7 × 7 × 10 cm) on an elevated mesh floor and allowed to habituate for 30 min before threshold testing. A logarithmic series of 8 calibrated Semmes-Weinstein monofilaments (von Frey hairs; Stoelting, Kiel, WI, USA) (0.008, 0.02, 0.04, 0.16, 0.4, 0.6, 1, 1.4, and 2 g) with various bending forces (0.078, 0.196, 0.392, 1.568, 3.92, 5.88, 9.8, 13.72, and 19.6 mN) was applied to the plantar surface of the hind paw until the mice withdrew from the stimulus. Positive responses included licking, biting, and sudden withdrawal of the hind paws. A von Frey filament was applied 5 times (3 seconds for each stimulus) to each tested area. The minimum bending force of the von Frey filament able to evoke 3 occurrences of the paw withdrawal reflex was considered the paw withdrawal threshold. All tests were performed in a blinded manner.

CatWalk gait analysis

Gait analysis was conducted using the CatWalk XT system (Noldus, the Netherlands) to measure pain-related parameters. The experimental setup involved placing the mouse on a glass platform with open ends, allowing the mouse to walk voluntarily. Simultaneously, a high-speed camera positioned underneath the platform captured images of each step, which were then transmitted to the analysis software (version 10.6, CatWalk XT, Noldus) for further processing. In this study, eight parameters were identified to assess dynamic behaviors relevant to neuropathic pain: (1) Stand: this parameter represents the duration (in seconds) of a paw touching the glass plate; (2) Stand index: it describes the speed at which the paw moves away from the glass plate; (3) Max contact area: it describes the maximum contact area of the paw or leg with the glass plate; (4) Mean print area: it represents the average area of the paw print during locomotion; (5) Mean intensity: this parameter denotes the average intensity value of the running stage; (6) Duty cycle This parameter denotes the average intensity value of the running stage.

Statistical Analysis

GraphPad Prism 5 (Graph Pad Software, Inc.) was used for the statistical analyses and graphing. Statistical significance was assessed by unpaired *t*-test, paired *t*-test, one-way and two-way ANOVA followed by *post hoc* comparison, Wilcoxon matched-paired signed rank test and Mann-Whitney test. All data in the experiment are expressed in mean ± S.E.M. Statistical significance was indicated as *, $P < 0.05$, **, $P < 0.01$, ***, $P < 0.001$ and ****, $P < 0.0001$.

Competing interests

The authors declare there are no conflicts of interest/competing interests related to this work.

Author contributions

W.-Y.P., Data curtation, Formal analysis, Investigation, Visualization, Writing-original draft, Writing-review and editing, Funding acquisition; P.W., Data curation, Investigation, Methodology; C.-Y.T., Data curation, Investigation, Methodology, Writing-original draft; H.Z., Investigation, Methodology; K.C., Investigation; H.-X.S., Methodology; Y.-C.T., Methodology; A.-X.L., Methodology; Z.Z., Investigation, software; Y.-F.Y., Investigation; K.-J.W., Data curation, Investigation, Methodology, Writing-original draft; C.C., Conceptualization, Supervision; Y.-M.W., Supervision, Investigation, Methodology; T.C., Conceptualization, Supervision, Funding acquisition, Investigation, Visualization, Methodology, Writing-review and editing, Project administration, Funding acquisition.

Acknowledgements

We thank the support the teaching center of Air force medical university for the invaluable technical assistance and J.-X.G. of our laboratory for the helpful comments on an earlier version of the manuscript and discussions. This work was supported by grants from the National Natural Science Foundation of China (32192410, 32071000 to T. C., 82271893 to Y.-M.W., 8230071226 to W.-Y.P., 82302090 to K.C.), National Science Fund for Distinguished Young Scholars (12225511 to C.C.), National Science Fund of China Major Project (T2241002 to C.C.), Innovation Laboratory of Terahertz Biophysics (23-163-00-GZ-001-001-02-04 to W.-Y.P.), The Key Research and Development Plan of Shaanxi Province (S2024-YF-YBSF-0277 to W.-Y.P.)

References

1. Baron R., Binder G. (2010) **A Fau - Wasner, G. Wasner, Neuropathic pain: diagnosis, pathophysiological mechanisms, and treatment** *The Lancet. Neurology* **9**:807–819

2. Shan L., Selvarajah D., Wang Z. (2023) **Editorial: Insights in neuropathic pain: 2022** *Frontiers in pain research (Lausanne, Switzerland)* **4**

3. Jensen T. S., Finnerup N. B. (2014) **Allodynia and hyperalgesia in neuropathic pain: clinical manifestations and mechanisms** *The Lancet. Neurology* **13**:924–935

4. Costigan M., Scholz C. J. (2009) **J Fau - Woolf, C. J. Woolf, Neuropathic pain: a maladaptive response of the nervous system to damage** *Annual review of neuroscience* **32**:1–32

5. Liu K., Wang L. (2019) **Optogenetics: Therapeutic spark in neuropathic pain** *Bosnian journal of basic medical sciences* **19**:321–327

6. Peng W., et al. (2023) **High-frequency terahertz waves disrupt Alzheimer's β-amyloid fibril formation** *eLight* **3**

7. Li Y., Chang C., Zhu Z., Fan C. (2021) **Terahertz Wave Enhances Permeability of the Voltage-Gated Calcium Channel** *Journal of the American Chemical Society* **143**:4311–4318

8. Zhao Y., Wang L., Li Y., Zhu Z. (2023) **Terahertz Waves Enhance the Permeability of Sodium Channels** *Symmetry* **15**

9. Zhang J., et al. (2021) **Non-invasive, opsin-free mid-infrared modulation activates cortical neurons and accelerates associative learning** *Nature Communications* **12**

10. Liu X., Qiao Z., Chai Y., Zhu Z., et al. (2021) **Nonthermal and reversible control of neuronal signaling and behavior by midinfrared stimulation** *Proceedings of the National Academy of Sciences of the United States of America* **118**

11. Trimmer J. S. (2014) **Ion channels and pain: important steps towards validating a new therapeutic target for neuropathic pain** *Experimental neurology* **254**:190–194

12. Bliss T. V. P., Collingridge G. L., Kaang B.-K., Zhuo M. (2016) **Synaptic plasticity in the anterior cingulate cortex in acute and chronic pain** *Nature Reviews Neuroscience* **17**:485–496

13. Tsuda M. A.-O., Koga K., Chen T., Zhuo M. (2017) **Neuronal and microglial mechanisms for neuropathic pain in the spinal dorsal horn and anterior cingulate cortex** *Journal of neurochemistry* **141**:486–498

14. Chen W., T Fau - Wang, et al. (2014) **, Postsynaptic insertion of AMPA receptor onto cortical pyramidal neurons in the anterior cingulate cortex after peripheral nerve injury** *Molecular brain* **7**

15. Koga K., et al. (2015) **Coexistence of two forms of LTP in ACC provides a synaptic mechanism for the interactions between anxiety and chronic pain** *Neuron* **85**:377–389

16. Chen T., et al. (2018) **Top-down descending facilitation of spinal sensory excitatory transmission from the anterior cingulate cortex** *Nature communications* **9**

17. Alles S. R. A., Smith P. A. (2018) **Etiology and Pharmacology of Neuropathic Pain** *Pharmacological reviews* **70**:315–347

18. Bliss T. V., Collingridge G. L., Kaang B. K., Zhuo M. (2016) **Synaptic plasticity in the anterior cingulate cortex in acute and chronic pain** *Nature reviews. Neuroscience* **17**:485–496

19. Zhu D. Y., et al. (2022) **The increased in vivo firing of pyramidal cells but not interneurons in the anterior cingulate cortex after neuropathic pain** *Molecular brain* **15**

20. Li X.-Y., et al. (2010) **Alleviating Neuropathic Pain Hypersensitivity by Inhibiting PKMζ in the Anterior Cingulate Cortex** *Science* **330**:1400–1404

21. Kang S. J., et al. (2015) **Bidirectional modulation of hyperalgesia via the specific control of excitatory and inhibitory neuronal activity in the ACC** *Molecular Brain* **8**

22. Fuchs P. N., Peng Y. B., Boyette-Davis J. A., Uhelski M. L. (2014) **The anterior cingulate cortex and pain processing** *Frontiers in integrative neuroscience* **8**

23. Lançon K., Qu C., Navratilova E., Porreca F., Séguéla P. (2021) **Decreased dopaminergic inhibition of pyramidal neurons in anterior cingulate cortex maintains chronic neuropathic pain** *Cell reports* **37**

24. Um S. W., Kim M. J., Leem J. W., Bai S. J., Lee B. H. (2019) **Pain-Relieving Effects of mTOR Inhibitor in the Anterior Cingulate Cortex of Neuropathic Rats** *Molecular Neurobiology* **56**:2482–2494

25. Tan W., et al. (2015) **Alleviating neuropathic pain mechanical allodynia by increasing Cdh1 in the anterior cingulate cortex** *Molecular pain* **11**

26. Takeda M., et al. (2011) **Potassium channels as a potential therapeutic target for trigeminal neuropathic and inflammatory pain** *Molecular pain* **7**

27. Du X., Gamper N. (2013) **Potassium channels in peripheral pain pathways: expression, function and therapeutic potential** *Current neuropharmacology* **11**:621–40

28. Sakai A., et al. (2017) **MicroRNA cluster miR-17-92 regulates multiple functionally related voltage-gated potassium channels in chronic neuropathic pain** *Nature Communications* **8**

29. Zhao J.-Y., et al. (2017) **DNA methyltransferase DNMT3a contributes to neuropathic pain by repressing Kcna2 in primary afferent neurons** *Nature Communications* **8**

30. Fan L., et al. (2014) **Impaired neuropathic pain and preserved acute pain in rats overexpressing voltage-gated potassium channel subunit Kv1.2 in primary afferent neurons** *Molecular Pain* **10**

31. Tsantoulas C., McMahon S. B. (2014) **Opening paths to novel analgesics: the role of potassium channels in chronic pain** *Trends in neurosciences* **37**:146–158

32. Khandelwal N. A.-O., et al. (2021) **FOXP1 negatively regulates intrinsic excitability in D2 striatal projection neurons by promoting inwardly rectifying and leak potassium currents** *Molecular psychiatry* **26**:1761–1774

33. González C., et al. (2012) **K(+) channels: function-structural overview** *Comprehensive Physiology* **2**:2087–2149

34. Zhang K. L., et al. (2022) **Targeted up-regulation of Drp1 in dorsal horn attenuates neuropathic pain hypersensitivity by increasing mitochondrial fission** *Redox biology* **49**

35. Zhao R., et al. (2018) **Neuropathic Pain Causes Pyramidal Neuronal Hyperactivity in the Anterior Cingulate Cortex** *Frontiers in cellular neuroscience* **12**

36. Chen Z., Shen X., Huang L., Wu H., Zhang M. (2018) **Membrane potential synchrony of neurons in anterior cingulate cortex plays a pivotal role in generation of neuropathic pain** *Scientific Reports* **8**

37. Xu H., et al. (2008) **Presynaptic and postsynaptic amplifications of neuropathic pain in the anterior cingulate cortex** *The Journal of neuroscience: the official journal of the Society for Neuroscience* **28**:7445–7453

38. Gao K., Lin Z., Wen S., Jiang Y. (2022) **Potassium channels and epilepsy** *Acta neurologica Scandinavica* **146**:699–707

39. Maljevic S., Lerche H. (2013) **Potassium channels: a review of broadening therapeutic possibilities for neurological diseases** *Journal of neurology* **260**:2201–2211

40. Al-Sabi A., Kaza Seshu K., Dolly J. O., Wang J. (2013) **Pharmacological characteristics of Kv1.1- and Kv1.2-containing channels are influenced by the stoichiometry and positioning of their α subunits** *Biochemical Journal* **454**:101–108

41. Liang Y., et al. (2024) **Transcription factor EBF1 mitigates neuropathic pain by rescuing Kv1.2 expression in primary sensory neurons** *Translational research: the journal of laboratory and clinical medicine* **263**:15–27

42. Zhang J., et al. (2021) **Epigenetic restoration of voltage-gated potassium channel Kv1.2 alleviates nerve injury-induced neuropathic pain** *Journal of neurochemistry* **156**:367–378

43. Xiao T. A.-O., et al. (2023) **Sensory input-dependent gain modulation of the optokinetic nystagmus by mid-infrared stimulation in pigeons** *eLife* **12**

44. Xiao X., Zhang Y.-Q. (2018) **A new perspective on the anterior cingulate cortex and affective pain** *Neuroscience & Biobehavioral Reviews* **90**:200–211

45. Kang S. J., et al. (2015) **Bidirectional modulation of hyperalgesia via the specific control of excitatory and inhibitory neuronal activity in the ACC** *Molecular brain* **8**

46. Cichon J., Blanck T. J. J., Gan W.-B., Yang G. (2017) **Activation of cortical somatostatin interneurons prevents the development of neuropathic pain** *Nature Neuroscience* **20**:1122–1132

47. Zhou R., Wang W. (2019) **C Fau - Xu, L. Xu W Fau - Xie, L. Xie, Biological applications of terahertz technology based on nanomaterials and nanostructures** *Nanoscale* **11**:3445–3457

48. Wang Q., Chen Y., Mao J., Yang F., Wang N. A.-O. (2023) **Metasurface-Assisted Terahertz Sensing** *Sensors (Basel, Switzerland)* **23**

49. Cole B. A., Clapcote S. J., Muench S. P., Lippiat J. D. (2021) **Targeting K(Na)1.1 channels in KCNT1-associated epilepsy** *Trends in pharmacological sciences* **42**:700–713

50. Jentsch T. J. (2000) **Neuronal KCNQ potassium channels: physiology and role in disease** *Neuroscience* **1**:21–30

51. Taylor J. L., et al. (2022) **Functionally linked potassium channel activity in cerebral endothelial and smooth muscle cells is compromised in Alzheimer's disease** *Proceedings of the National Academy of Sciences of the United States of America* **119**

52. Häusser M. (2000) **The Hodgkin-Huxley theory of the action potential** *Nature Neuroscience* **3**:1165–1165

53. Guo Z. V., et al. (2014) **Procedures for behavioral experiments in head-fixed mice** *PloS one* **9**

54. Zhang M. M., et al. (2022) **Glutamatergic synapses from the insular cortex to the basolateral amygdala encode observational pain** *Neuron* **110**:1993–2008

55. Apkarian A. V. (2005) **R.-D. Bushnell Mc Fau - Treede, J.-K. Treede Rd Fau - Zubieta, J. K. Zubieta, Human brain mechanisms of pain perception and regulation in health and disease** *European journal of pain (London, England)* **9**:463–484

Editors

Reviewer #1 (Public Review):

In this manuscript, by using simulation, in vitro and in vivo electrophysiology, and behavioral tests, Peng et al. nicely showed a new approach for the treatment of neuropathic pain in mice. They found that terahertz (THz) waves increased Kv conductance and decreased the frequency of action potentials in pyramidal neurons in the ACC region. Behaviorally, terahertz (THz) waves alleviated neuropathic pain in the mouse model. Overall, this is an interesting study. The experimental design is clear, the data is presented well, and the paper is well-written.

I have a few suggestions.
(1) The authors provide strong theoretical and experimental evidence for the impact of voltage-gated potassium channels by terahertz wave frequency. However, the modulation of action potential also relies on non-voltage-dependent ion channels. For example, I noticed that the RMP was affected by THz application (Fig. 3F) as well. As the RMP is largely regulated by the leak potassium channels (Tandem-pore potassium channels), I would suggest testing whether terahertz wave photons have also any impact on the Kleak channels as well.

(2) The activation curves of the Kv currents in Fig. 2h seem to be not well-fitted. I would suggest testing a higher voltage (>100 mV) to collect more data to achieve a better fitting.

(3) In the part of behavior tests, the pain threshold increased after THz application and lasted within 60 mins. I suggest conducting prolonged tests to determine the end of the analgesic effect of terahertz waves.

(4) Regarding in vivo electrophysiological recordings, the post-HFTS recordings were acquired from a time window of up to 20 min. It seems that the HFTS effect lasted for minutes, but this was not tested in vitro where they looked at potassium currents. This long-lasting effect of HFTS is interesting. Can the authors discuss it and its possible mechanisms, or test it in slice electrophysiological experiments?

(5) How did the authors arrange the fiber for HFTS delivery and the electrode for in vivo multi-channel recordings? Providing a schematic illustration in Fig. 4 would be useful.

(6) Language is largely OK, but some grammar errors should be corrected.

The authors have completely addressed my concerns. I have no further comments.

https://doi.org/10.7554/eLife.97444.2.sa3

Reviewer #2 (Public Review):

Summary:

In this manuscript, Peng et al., reported that 36THz high-frequency terahertz stimulation (HFTS) can suppress the activity of pyramidal neurons through enhancing the conductance of voltage-gated potassium channel. The authors also demonstrated the effectiveness of using 36THz HFTS for treating neuropathic pain.

Strengths:

The manuscript is well written and the conclusions are supported by robust results. This study highlighted the potential of using 36THz HFTS for neuromodulation.

Weaknesses:

More characterization of HFTS is needed, so the readers can have a better assessment of the potential usage of HFTS in their own applications.

https://doi.org/10.7554/eLife.97444.2.sa2

Reviewer #3 (Public Review):

My summary of the manuscript remains the same and is as follows:

This manuscript by Peng et al. presents intriguing data indicating that high-frequency terahertz stimulation (HFTS) of the anterior cingulate cortex (ACC) can alleviate neuropathic pain behaviors in mice. Specifically, the investigators report that terahertz (THz) frequency stimulation widens the selectivity filter of potassium channels thereby increasing potassium conductance leading to a reduction in the excitability of cortical neurons. In voltage clamp recordings from layer 5 ACC pyramidal neurons in acute brain slice, Peng et al. show that HFTS enhances K current while showing minimal effects on Na current. Current clamp recording analyses show that the spared nerve injury model of neuropathic pain decreases the current threshold for action potential (AP) generation and increases evoked AP frequency in layer 5 ACC pyramidal neurons, which is consistent with previous studies. Data are presented showing that ex-vivo treatment with HFTS in slice reduces these SNI-induced

changes to excitability in layer 5 ACC pyramidal neurons. The authors also confirm that HFTS reduces excitability of layer 5 ACC pyramidal neurons via in vivo multi-channel recordings from SNI mice. Lastly, the authors show that HFTS is effective at reducing mechanical allodynia in SNI using both the von Frey and Catwalk analyses. Overall, there is considerable enthusiasm for the findings presented in this manuscript given the need for non-pharmacological treatments for pain in the clinical setting.

https://doi.org/10.7554/eLife.97444.2.sa1

Author response:

The following is the authors' response to the original reviews.

> ***Reviewer #1 (Public Review):***
>
> *In this manuscript, by using simulation, in vitro and in vivo electrophysiology, and behavioral tests, Peng et al. nicely showed a new approach for the treatment of neuropathic pain in mice. They found that terahertz (THz) waves increased Kv conductance and decreased the frequency of action potentials in pyramidal neurons in the ACC region. Behaviorally, terahertz (THz) waves alleviated neuropathic pain in the mouse model. Overall, this is an interesting study. The experimental design is clear, the data is presented well, and the paper is well-written. I have a few suggestions.*
>
> *(1) The authors provide strong theoretical and experimental evidence for the impact of voltage-gated potassium channels by terahertz wave frequency. However, the modulation of action potential also relies on non-voltage-dependent ion channels. For example, I noticed that the RMP was affected by THz application (Figure 3F) as well. As the RMP is largely regulated by the leak potassium channels (Tandem-pore potassium channels), I would suggest testing whether terahertz wave photons have also any impact on the Kleak channels as well.*

Thank you for your positive comment and for providing us with this valuable suggestion. After testing the leak K+ current with and without HFTS on the SNI model, we observed a notable increase in the leak K+ current with HFTS when the holding potential surpassed -40 mV (please see the revised Figs. 2m and n). This finding prompted us to delve deeper into the shifts in the resting membrane potential (RMP). The data, along with statistical analysis, are detailed in Tables S1-3.

> *(2) The activation curves of the Kv currents in Figure 2h seem to be not well-fitted. I would suggest testing a higher voltage (>100 mV) to collect more data to achieve a better fitting.*

Thanks for your advice. We repeated the experiment while maintaining the voltage of patched neurons at a higher level (>100 mV) to collect ample data for better fitting. The outcomes are illustrated in the revised Figs. 2g-j. Clearly, the data reveals a significant increase in K+ conductance in the HFTS group as compared to the SNI group. We have integrated these discoveries into the revised manuscript, replacing the earlier results.

> *(3) In the part of behavior tests, the pain threshold increased after THz application and lasted within 60 mins. I suggest conducting prolonged tests to determine the end of the analgesic effect of terahertz waves.*

Thank you for your insightful comment. We echo your curiosity about the duration of the HFTS effect. In the process of revising our work, we conducted a comparative analysis of the

analgesic duration resulting from 10-minute and 15-minute applications of HFTS. The findings are visualized in the revised Fig. 5c. Our observations indicate that after 160 minutes, the PWMT value for the 15-minute HFTS group decreased to a level comparable to that of the SNI group. Meanwhile, the analgesic effects persisted for 140 minutes in the case of the 10-minute HFTS application. These results imply a direct correlation between the duration of HFTS application and the duration of analgesia.

> *(4) Regarding in vivo electrophysiological recordings, the post-HFTS recordings were acquired from a time window of up to 20 min. It seems that the HFTS effect lasted for minutes, but this was not tested in vitro where they looked at potassium currents. This long-lasting effect of HFTS is interesting. Can the authors discuss it and its possible mechanisms, or test it in slice electrophysiological experiments?*

Thank you for your comment. Based on the results from *in vivo* electrophysiological recordings, it was observed that the effect of HFTS can endure for a minimum of 20 minutes, and this duration was even more extended in behavioral assessments. Taking your advice, we employed slice electrophysiological recording for further testing. Following a 15-minute application of HFTS, we evaluated the K+ current at 5 and 20 minutes after incubation. Our observations clearly indicated a substantial and lasting increase in K+ current, with the effect persisting for at least 20 minutes (refer to Fig. 2l). This provides confirmation of the long-lasting influence of HFTS. The relevant data and statistical analysis are documented in Table S1-2.

> *(5) How did the authors arrange the fiber for HFTS delivery and the electrode for in vivo multi-channel recordings? Providing a schematic illustration in Figure 4 would be useful.*

Thank you for your comment. To enhance the reader's understanding of the HFTS delivery device during multi-channel recording, we have included a schematic illustration in Fig. 4a in the revised manuscript. The top portion of Fig. 4a depicts a quantum cascade laser (QCL) with a center frequency located at approximately 36 THz. This laser is then connected to the recording electrode via a PIR fiber. The left section illustrates the detailed structure of the recording electrode.

> *(6) Some grammatical errors should be corrected.*

Thank you for your thorough review. We have carefully checked and corrected grammar errors we found throughout the entire text to ensure that readers can better comprehend the content of the article.

> ***Reviewer #2 (Public Review):***
>
> *In this manuscript, Peng et al., reported that 36 THz high-frequency terahertz stimulation (HFTS) can suppress the activity of pyramidal neurons by enhancing the conductance of voltage-gated potassium channel. The authors also demonstrated the effectiveness of using 36THz HFTS for treating neuropathic pain.*
>
> *Strengths:*
>
> *The manuscript is well written and the conclusions are supported by robust results. This study highlighted the potential of using 36 THz HFTS for neuromodulation.*
>
> *Weaknesses:*
>
> *More characterization of HFTS is needed, so the readers can have a better assessment of the potential usage of HFTS in their own applications.*

Thank you for your suggestion. We have created schematic diagrams illustrating the HFTS delivery (Fig. 4a and Fig. 5a in the revised manuscript). Fig. 4a presents the structure designed for *in vivo* multi-channel recording. Fig. 5a shows the structure used in behavior test, the recording electrode is replaced by a metal hollow tube, allowing the PIR fiber to pass through the tube and target the ACC region of the mice.

> *(1) It would be very helpful to estimate the volume of tissue that can be influenced by HFTS. It is not clear how 15 mins HFTS was chosen for this functional study. Does a longer time have a stronger effect? A better characterization of the relationship between the stimulus duration of HFTS and its beneficial effects would be very useful.*

Thank you for your feedback. The degree of tissue influence is directly related to the size of the spot emerging from the fiber outlet. In our experiment, we used a PIR fiber with a 630 nm inner core diameter to propagate high-frequency THz waves. This core features a refractive index of 2.15 and has an effective numerical aperture (NA) of 0.35 ± 0.05.

Our decision to apply HFTS for 15 minutes in the behavioral study was primarily based on observations from *in vivo* multi-channel recordings. Specifically, we noticed a considerable reduction in the average firing rate of PYR cells after 15 minutes of HFTS exposure. To further investigate the correlation between the duration of HFTS stimulation and its effects, we conducted a comparative study using a 10-minute HFTS session. The results, depicted in revised Fig. 5c, reveal that the PWMT value decreased to the level seen in the SNI group after approximately 160 minutes following 15 minutes of HFTS, and after about 140 minutes with 10 minutes of HFTS. This suggests a direct relationship between the length of HFTS application and its beneficial outcomes.

> *(2) How long does the behavioral effect last after 15 minutes of HFTS? Figure 5b only presents the behavioral effect for one hour, but the pain level is still effectively reduced at this time point. The behavioral measurement should last until pain sensitization drops back to pre-stim level.*

Thank you for your feedback. Similar question is also mentioned by reviewer 1. As depicted in Fig. 5c, it was observed that the analgesic effects lasted for 140-160 min with 10-15 minutes application of HFTS. Based on these findings, we can conclude that in the SNI model, targeting the ACC brain region with HFTS for a duration of 10-15 minutes results in an analgesic effect that lasts for roughly 140-160 minutes. This provides valuable insights into the potential clinical applications and duration of relief that can be achieved through HFTS treatment.

> *(3) Although the manuscript only tested in ACC, it will also be useful to demonstrate the neural modulation effect on other brain regions. Would 36THz HFTS also robustly modulate activities in other brain regions? Or are different frequencies needed for different brain regions?*

Thank you for your comment. We hypothesize that light waves at a frequency of approximately 36 THz effectively modulate neuronal activities in various brain regions, primarily due to their impact on K channels. Additionally, we speculate that the application of THz waves at different frequencies may influence other channels, such as Na and Ca channels, potentially facilitating or inhibiting neuronal activities. We believe this is a fascinating and significant area of research to explore in the future.

> ***Reviewer #3 (Public Review):***
>
> *Summary:*

> *This manuscript by Peng et al. presents intriguing data indicating that high-frequency terahertz stimulation (HFTS) of the anterior cingulate cortex (ACC) can alleviate neuropathic pain behaviors in mice. Specifically, the investigators report that terahertz (THz) frequency stimulation widens the selectivity filter of potassium channels thereby increasing potassium conductance and leading to a reduction in the excitability of cortical neurons. In voltage clamp recordings from layer 5 ACC pyramidal neurons in acute brain slice, Peng et al. show that HFTS enhances K current while showing minimal effects on Na current. Current clamp recording analyses show that the spared nerve injury model of neuropathic pain decreases the current threshold for action potential (AP) generation and increases evoked AP frequency in layer 5 ACC pyramidal neurons, which is consistent with previous studies. Data are presented showing that ex-vivo treatment with HFTS in slice reduces these SNI-induced changes to excitability in layer 5 ACC pyramidal neurons. The authors also confirm that HFTS reduces the excitability of layer 5 ACC pyramidal neurons via in vivo multi-channel recordings from SNI mice. Lastly, the authors show that HFTS is effective at reducing mechanical allodynia in SNI using both the von Frey and Catwalk analyses. Overall, there is considerable enthusiasm for the findings presented in this manuscript given the need for non-pharmacological treatments for pain in the clinical setting.*
>
> *Strengths:*
>
> *The authors use a multifaceted approach that includes modeling, ex-vivo and in-vivo electrophysiological recordings, and behavioral analyses. Interpretation of the findings is consistent with the data presented. This preclinical work in mice provides new insight into the potential use of directed high-frequency stimulation to the cortex as a primary or adjunctive treatment for chronic pain.*
>
> *Weaknesses:*
>
> *There are a few concerns noted that if addressed, would significantly increase enthusiasm for the study.*
>
> *(1) The left Na current trace for SNI + HFTS in Figure 2B looks to have a significant series resistance error. Time constants (tau) for the rate of activation and inactivation for Na currents would be informative.*

Thank you for your feedback. We have carefully considered your comments and made several adjustments in the revised Figs. 2b-f to improve clarity and accuracy. Firstly, we have conducted a comparison of the time constants (tau) between the SNI group and the SNI+HFTS group. These time constants represent the latency of Na current activation or inactivation relative to the half-activated/inactivated voltage. Our analysis reveals that there is no statistically significant difference in tau between the two groups for both activation and deactivation curves. Secondly, we have updated the sample traces in Fig. 2b of the revised manuscript. These new traces illustrate that tau does not significantly differ between the SNI and SNI+HFTS groups, providing a visual representation of our findings. We believe that these modifications strengthen the presentation of our study's details and results, making the data more accessible and understandable for readers.

> *(2) It is unclear why an unpaired t-test was performed for paired data in Figure 2. Also, statistical methods and values for non-significant data should be presented.*

Thank you for your comment. I think you mean the results in Fig. 3. We agree with you that we should use one-way ANOVA to analyze the data since there are more than 2 groups for comparison. We thus re-analyzed the data by using one-way ANOVA in Figs. 3g-k, and have included detailed statistical methods and *P* values in the revised manuscript.

> *(3) It would seem logical to perform HFTS on ACC-Pyr neurons in acute slices from sham mice (i.e. Figure 3 scenario). These experiments would be informative given the data presented in Figure 4.*

Thank you for your valuable advice. During the revision process, we performed HFTS on ACC-PYR neurons in acute slices obtained from sham mice. The findings from this experiment have been integrated into the updated Fig. 3, where the sham group is represented by the green line and histogram (the revised Fig. 3 in the manuscript). It is noteworthy that a significant decrease in spike frequency was observed in the sham mice following HFTS.

> *(4) As the data are presented in Figure 4g, it does not seem as if SNI significantly increased the mean firing rate for ACC-Pyr neurons, which is observed in the slice. The data were analyzed using a paired t-test within each group (sham and SNI), but there is no indication that statistical comparisons across groups were performed. If the argument is that HFTS can restore normal activity of ACC-Pyr neurons following SNI, this is a bit concerning if no significant increase in ACC-Pyr activity is observed in in-vivo recordings from SNI mice.*

Thank you for highlighting the inaccuracies in the analysis. After reviewing the data, we re-analyzed it using alternative statistical methods. In the revised version, since the data did not follow a normal distribution, we employed Wilcoxon matched-paired signed rank tests within the sham and SNI groups, and Mann-Whitney tests between the sham and SNI groups.

Upon comparing the statistical outcomes across the groups, we found that the mean firing rate of 130 ACC neurons in SNI mice was significantly higher compared to that of 108 ACC neurons in sham mice (P = 0.0447, Mann-Whitney test). Notably, the mean firing rate of ACC-PYR exhibited a more pronounced increase with a P value of 0.0274 in SNI pre-HFTS versus sham pre-HFTS, while the mean firing rate of ACC-INT did not display a significant change across the groups. These findings align with the observations we made in the slice, reinforcing the validity of our results.

> *(5) The authors indicate that the effects of HFTS are due to changes in Kv1.2. However, they do not directly test this. A blocking peptide or dendrotoxin could be used in voltage clamp recordings to eliminate Kv1.2 current and then test if this eliminates the effects of HFTS. If K current is completely blocked in VC recordings then the authors can claim that currents they are recording are Kv1.1 or 1.2.*

Thank you for your kind suggestion. In our research, we employed the Kv1.2 structure as a model to determine the response frequency of terahertz waves. Through both *in vitro* and *in vivo* experiments, we were able to demonstrate that the frequency of approximately 36 THz affects the Kv channel and its corresponding spike frequency. Upon analyzing the action potential waveform, we observed a notable variance in the resting membrane potential (RMP). This RMP is predominantly controlled by leak potassium channels, specifically the Tandem-pore potassium channels. In accordance with the recommendation of reviewer 1, we have addressed this particular aspect of our experimentation in the revised manuscript.

We agree that we should use blocking peptides or dendrotoxin to eliminate Kv1.2 current. However, we meet problems in purchasing and delivery of the drugs. We thus added some explanation in the Discussion part to emphasize the value for this pharmacological experiment and can further confirm this in the future works.

> *(6) The ACC is implicated in modulating the aversive aspect of pain. It would be interesting to know whether HFTS could induce conditioned place preference in SNI mice*

> *via negative reinforcement (i.e. alleviation of spontaneous pain due to the injury). This would strengthen the clinical relevance of using HFTS in treating pain.*

Thank you for this valuable advice. We share your intrigue regarding this experiment, and we fully recognize the importance and potential of further exploring this area. At present, however, our equipment and platform limitations prevent us from conducting the necessary tests. However, we remain committed to pursuing relevant research opportunities in the future.

https://doi.org/10.7554/eLife.97444.2.sa0